New Configuration of Solid-State Neutron Detector Made Possible with Solution-Based Semiconductor Processing

*Huiqiong Zhou, Nelson E. Coates, Gerardo Hernandez-Sosa, and Daniel Moses**

The unique benefit of solution-based fabrication of solid-state p-n junctions is demonstrated for radiation detection. In particular, an in situ inorganic semiconductor synthesis and film deposition facilitates a novel neutron detector configuration consisting of a host inorganic semiconductor matrix impregnated with a guest neutron sensitizing material. Spectroscopic investigations of the structural order of the top detector active layer indicate that it consists of interpenetrating networks of the host semiconductor nanocrystals and sensitizing guest material that self-assemble during film formation. The host semiconductor network exhibits a good charge transport as evidenced by steady-state photoconductivity measurements. The detectors developed indicate high sensitivity to ionizing radiation and a demonstrated ability to detecting thermal neutrons.

1. Introduction

The development of solution-based inorganic semiconductor synthesis and film deposition techniques is typically driven by the goal of achieving a low cost device fabrication. However, for some device applications the solution-based approach enables a new device configuration that improves its inherent operation. Here we present a solution-based inorganic semiconductor synthesis, and demonstrate its utility for the fabrication of improved solid-state neutron detectors.

Solid-state neutron detectors have been the subject of extensive investigation in recent years due to the global shortage of ^{3}He.[1,2] In particular, low cost fabrication of solid-state neutron detectors would be useful for combating threats related to trafficking of illicit radiological materials and nuclear weapons.[3–5] Because of their charge neutrality, neutrons are notoriously difficult to detect directly, and thus nearly all neutron detection begins by a neutron capture in a nucleus of certain isotopes (e.g. ^{10}B) that undergo a fission reaction followed by generation of charged reaction products that in turn generate the optical or electronic detection signal.[6]

Many solid state neutron detector designs have been proposed that are based on the concept of coating a p-n junction with a layer of neutron sensitizing material (a converter layer) made of materials containing isotopes such as ^{6}Li or ^{10}B that are characterized by high capture cross-section for thermal neutrons, and subsequent fission decay that releases charged particles.[7–9] However, the detection efficiency of such detectors with a planar geometry is limited due to a tradeoff between the opposing requirements of high neutron capture efficiency (that favors a thick converter layer) and a high carrier excitation density in the p-n junction (that favors a thin converter layer). This tradeoff limits the detection efficiencies to about 3% in Si-based p-n junctions.[10] Attempts to improve device efficiency by using a non-planar p-n junction geometry (fabricated by etching array of holes[11] or parallel pillars[12–14] in Si substrate) are promising. For example, by increasing the pillar height from 12 μm to 26 μm, thermal neutron detection efficiency enhanced from 7%[12] to 20%.[13] However, this method generally requires more elaborate processing that lead to a significantly higher fabrication cost. Additionally, the detector overall cross-section area is limited due to the relatively high effective junction area with its resulted high capacitance that leads to enhanced detection noise. In the following we demonstrate a novel neutron detector configuration created via solution-based semiconductor processing that naturally solves some of the inherent issues involved with incorporating a neutron sensitizing material into a solid-state device.

2. Results and Discussion

Solution-based device fabrication has been extensively studied during the past decade.[15–17] Inorganic semiconductor devices that have been fabricated via solution processing include field effect transistors,[18] photodetectors,[19] and photovoltaics.[20] The most established device routes use a solution of colloidal quantum dots, which involves several processing steps.[21] First, quantum dots are nucleated from a homogeneous precursor solution. Following a controlled growth of these nucleated quantum dots they are isolated from solution and deposited on a substrate; finally, post-processing steps are performed to improve the electrical properties of the deposited semiconductor film.[17,22] The approach we developed utilizes an in situ inorganic semiconductor synthesis and film deposition that contains many of the benefits of colloidal quantum dot syntheses, but circumvents the use of electrically insulating ligands that lead to poor electrical performance in the films.[23,24] This

Dr. H. Q. Zhou, Dr. N. E. Coates,
Dr. G. Hernandez-Sosa, Dr. D. Moses
Center for Polymers and Organic Solids
University of California Santa Barbara
Santa Barbara, CA 93106-5090, USA
E-mail: moses@cpos.ucsb.edu

DOI: 10.1002/adfm.201200097

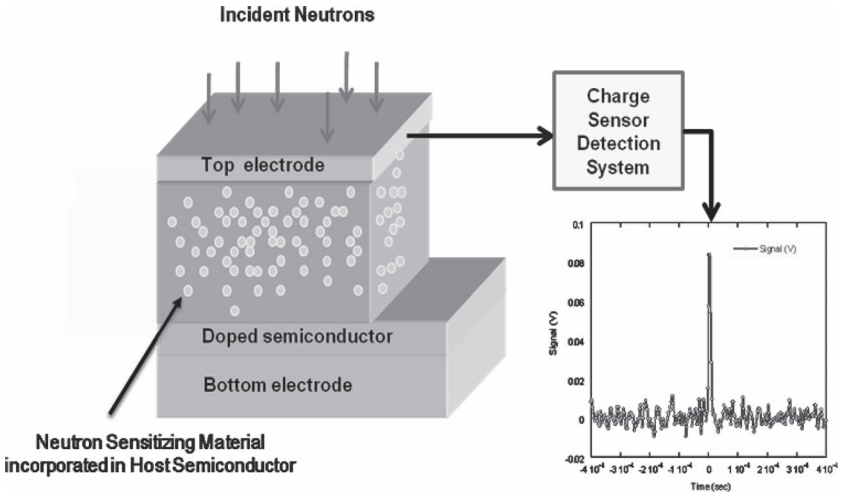

Figure 1. Schematic diagram of the neutron detectors developed using solution-based semiconductor processing.

simple synthesis results in a neutron detector top active layer that comprises a composite of host semiconductor (^{114}CdS) and neutron sensitizing compound ($^{10}B_2O_3$). This composite is deposited on p-doped Si wafer in order to create ^{114}CdS/Si p-n junction using a common solution containing ^{114}CdS precursor molecules and $^{10}B_2O_3$. The p-n junction is created at the ^{114}CdS/p-Si interfacial region (a system that was used for photovoltaic device applications as well).[25,26] This non-vacuum fabrication route is appealing because the neutron sensitizing material can be dispersed throughout the ^{114}CdS host semiconductor simply by incorporating the neutron sensitizing precursor molecules in the common starting solution of the semiconductor precursor molecules. **Figure 1** exhibits a schematic diagram of the detector system that indicates the structure of the top detector active layer.

Similarly to other sensitized neutron detectors,[11–14] the detection process starts with a neutron capture in one of the boron atoms in the ^{114}CdS:$^{10}B_2O_3$ top layer that triggers the follwing fission reaction: $n + {}^{10}B \rightarrow \alpha + {}^{7}Li$, resulting in byproducts of α particles with 1.47 MeV and ^{7}Li ions with 0.84 MeV. These charged particles propagate through the top layer during which they excite electron-hole pairs in the host semiconductor (CdS). Once the excited carriers diffuse into the p-n junction interfacial region, a current pulse is generated.

Briefly, for the in situ synthesis and fabrication of the detector top active layer ^{114}CdS:$^{10}B_2O_3$ film, we prepared a precursor solution containing $^{114}CdCl_2$, thiourea and $^{10}B_2O_3$ (99% enriched with ^{10}B) in a butylamine that acts as a solvent and a ligand for nucleating the semiconductor nanoparticles. The solution was drop-casted onto a freshly etched silicon wafer that was held at predetermined temperature of 150 °C in order to eliminate the volatile butylamine solvent as well as initiate a nucleation of ^{114}CdS nanoparticles. Following the drop-casting the temperature of the Si wafer was elevated to 450 °C to accelerate the nanoparticle synthesis, initiate a sintering of the ^{114}CdS colloids while they are small,[27] and eliminate the synthesis reaction byproducts.

An important feature of this solution-based fabrication approach is the spontaneous self-assembly of interpenetrating networks of the host semiconductor and the sensitizing guest material that are created during film formation, as is evident from the following observations. **Figure 2**a displays a scanning electron microscope (SEM) top view of pure ^{114}CdS film which indicates a porous structure of the semiconductor, possibly created by decomposition and elimination of the volatile surface ligands and precursor materials[23] during the post-film deposition heating treatment. Figure 2b displays the cross-section view of a neutron detector with active layer made of a composite of ^{114}CdS:$^{10}B_2O_3$ deposited from a solution; the bottom layer is a p-doped Si wafer and the top layer is an Al electrode. The latter SEM image suggests that the ^{114}CdS:$^{10}B_2O_3$ film is denser than the ^{114}CdS film, possibly due to a filling of the voids in the ^{114}CdS host semiconductor by the $^{10}B_2O_3$ neutron sensitizing material. Secondary ion mass spectrometry depth profile of ^{114}CdS:$^{10}B_2O_3$ composite film shown in Figure S1 indicates a homogenous distribution of $^{10}B_2O_3$ throughout the ^{114}CdS matrix. A third indication that confirms the existence of a phase separation of the semiconductor and neutron sensitizing components is exhibited by the XRD spectra of solution-deposited ^{114}CdS and ^{114}CdS:$^{10}B_2O_3$ films, shown in **Figure 3**. The XRD spectrum of pristine ^{114}CdS film indicates a hexagonal symmetry (P63mc space group, ICDD reference: 00-006-0314), and the spectrum of the ^{114}CdS:$^{10}B_2O_3$ film validates that this crystalline order of the ^{114}CdS component is retained in this composite.

A tendency for the nucleation of nanocrystals in one component is required for phase separation to occur, and for the ^{114}CdS:$^{10}B_2O_3$ composite, the ^{114}CdS component evidently manifests such tendency. Since the melting temperature of $^{10}B_2O_3$ (450 °C) is comparable to the temperature used for the final heat

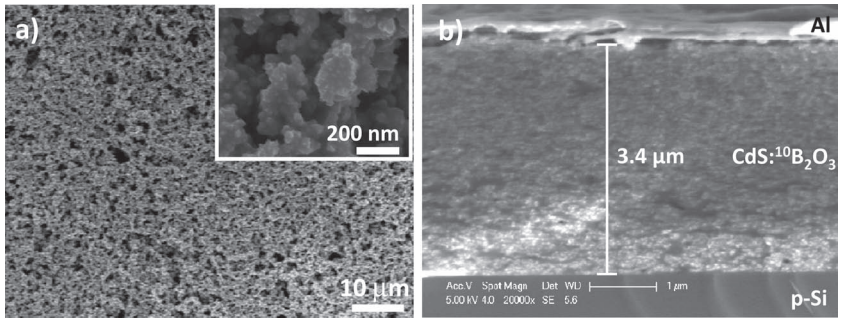

Figure 2. SEM images: a) top view of pure ^{114}CdS film; the inset shows a magnified image; b) cross-section view of neutron detector with an active layer made of a composite of ^{114}CdS:$^{10}B_2O_3$ deposited from a solution; the bottom layer is a p-doped Si wafer and the top layer is an Al electrode.

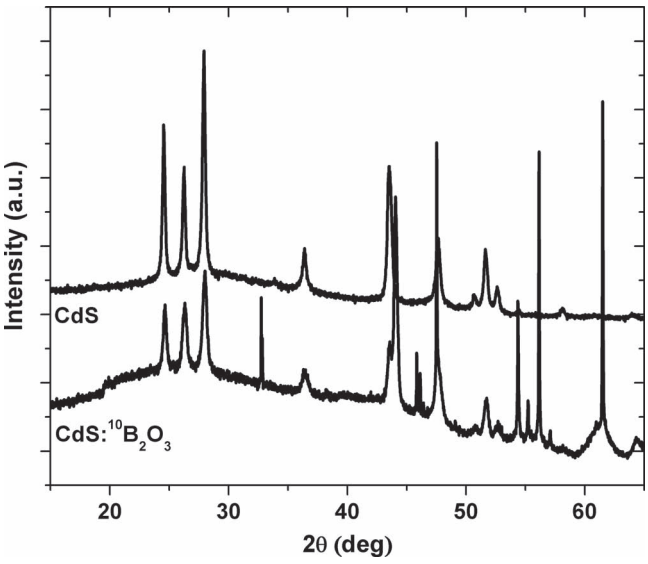

Figure 3. XRD spectra of pristine ^{114}CdS film (top curve) and ^{114}CdS:$^{10}B_2O_3$ composite film composed of 40% volume content of $^{10}B_2O_3$ (bottom curve) that was deposited from solution.

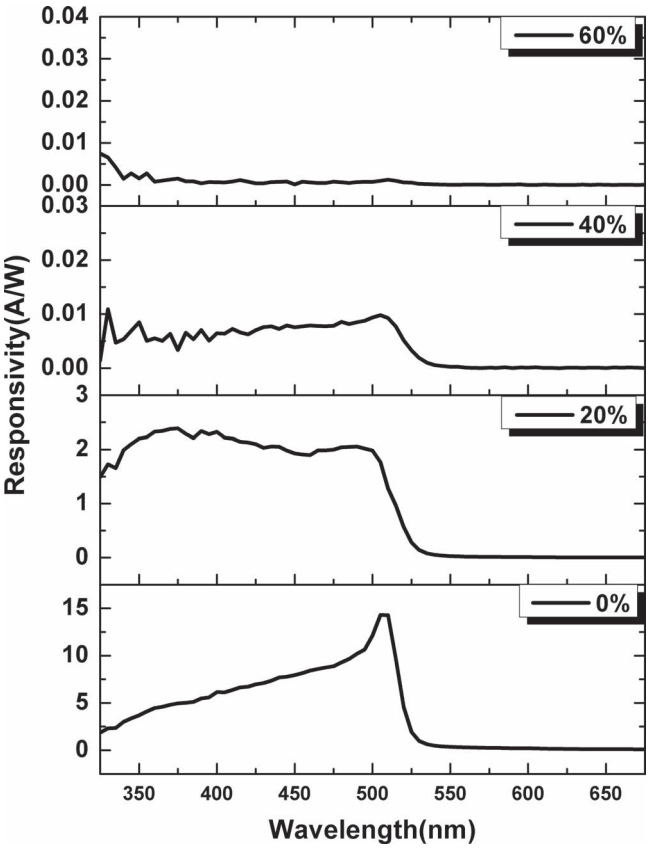

Figure 4. Steady-state photocurrent measurement of pristine ^{114}CdS film as well as ^{114}CdS:$^{10}B_2O_3$ composite films with different volume content of $^{10}B_2O_3$.

treatment processing step, it is likely that the ^{114}CdS nanoparticles grew and sintered into a network of polycrystalline ^{114}CdS in a liquid phase of $^{10}B_2O_3$.

This phase separated and interpenetrating network morphology in the top heterojunction layer facilitates a high carrier excitation density in the host semiconductor arising from the ^{10}B decay reaction products (^{7}Li and α particle) due to the spatial proximity of the neutron sensitizing compound and host semiconductor throughout the top detector active layer. Additionally, the continuous path of the semiconductor facilitates high collection efficiency of the excited carriers. The excitation paths of the secondary particles created in the ^{114}CdS:$^{10}B_2O_3$ composite following a neutron capture were estimated to be about 10 μm for the α particles generated with 1.47 MeV and about 5 μm for the ^{7}Li ions generated with 0.84 MeV, lengths which are on the order of the thickness of the ^{114}CdS:$^{10}B_2O_3$ top layers used (3 μm to 10 μm).

For attaining a good neutron detector performance, an optimal balance must be reached between neutron capture cross-section (which favors high volume content of the $^{10}B_2O_3$ insulator in the composite) and charge transport (which favors a smaller amount of $^{10}B_2O_3$ in the composite). Additionally, the top heterojunction layer thickness plays a role in determining the detector performance; an increase in thickness increases the neutron capture cross section, but decreases the number of carriers that are likely to reach the p-n junction. The optimum top heterojunction layer thickness is therefore determined by the carrier diffusion length in the ^{114}CdS:$^{10}B_2O_3$ film. Our experiments indicated an optimal detector performance (i.e., count rate) for device thickness ranging between 3 and 10 μm. Devices with larger thickness exhibited reduced detector pulse height, most likely due to reduced carrier collection efficiency through the thicker detector top active layer.

In order to determine the dependence of charge transport on the content of $^{10}B_2O_3$ in the ^{114}CdS:$^{10}B_2O_3$ composite film, planar steady-state photoconductivity measurements were taken on ^{114}CdS:$^{10}B_2O_3$ films comprising various volume contents of $^{10}B_2O_3$, and these results are shown in **Figure 4**. The pristine ^{114}CdS film exhibits high photoconductive responsivity, reaching 15 A/W when illuminated with 500 nm light and biased with 10^3 V/cm. This high responsivity indicates that good carrier transport is achieved by this in situ synthesis and film deposition route. The photoconductive responsivity of the ^{114}CdS:$^{10}B_2O_3$ composite film decreases monotonically with an increasing the $^{10}B_2O_3$ volume fraction. When the volume ratio of $^{10}B_2O_3$ reaches 40%, the photoconductive responsivity reduced by three orders of magnitude compared to the responsivity exhibited by ^{114}CdS, but its spectrum still displays the onset of the photocurrent near 520 nm. For the neutron detector device application we have used ^{114}CdS:$^{10}B_2O_3$ composite with 40% volume content of $^{10}B_2O_3$ that maintains a good balance between neutron capture efficiency and charge transport efficiency.

Manifestation of a ^{114}CdS:$^{10}B_2O_3$/Si p-n heterojunction is indicated with a measurement of the current versus applied bias, shown in **Figure 5**. The top active layer in this junction comprised ^{114}CdS:$^{10}B_2O_3$ layer with 40% volume content of $^{10}B_2O_3$. This device exhibits an increase in the current by almost 3 orders magnitude at a forward bias of 0.5 V.

The response of the solution-processed detectors to ionizing radiation was determined by irradiating them with 5.3 MeV α

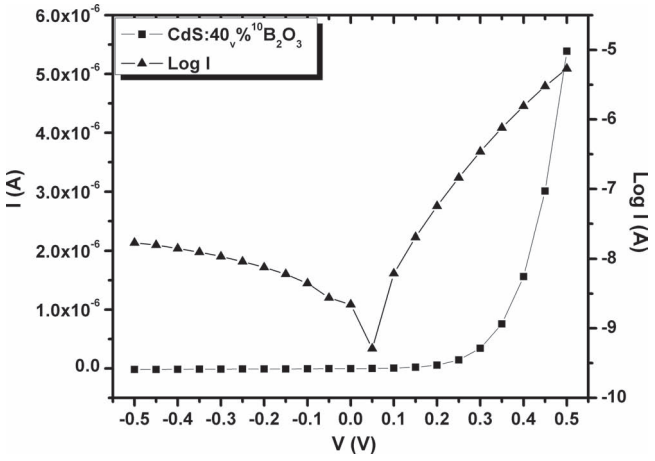

Figure 5. Dependence of the current on applied bias obtained from a $^{114}CdS:^{10}B_2O_3$/p-Si detector in which the top active layer is composed of 40% volume content of $^{10}B_2O_3$.

particles emitted from ^{210}Po source. A waterfall plot of the MCA spectral response of a $^{114}CdS:^{10}B_2O_3$/Si device (40% volume $^{10}B_2O_3$, ~3 μm top layer) with and without being exposed to a ^{210}Po source are shown in **Figure 6**. The Gaussian distribution of counts centered near bin 140 for this device indicates high detection efficiency for α particles, because even particles that caused a small number of collected carriers (low bin number) could be detected. To verify this high detection efficiency, a single crystal silicon diode detector was substituted for the solution-processed device, and although the voltage peak heights obtained from the mono-crystalline silicon device were higher, the total number of counts was nearly the same as that obtained from the device fabricated via solution processing. This similar total number of counts in conjunction with measurement of the α particles emission rate of the ^{210}Po source indicated the neutron-sensitized device detection efficiency for these a particles approaches 100%.

Finally, exposing this detector to neutron and gamma ray sources unambiguously indicated its capability of detecting thermal neutrons; the measured thermal neutron detection efficiency was about 10% of the maximum theoretical efficiency expected of this detector, and the detector discrimination ratio of gamma rays was greater than 10^4.

Our estimates indicate theoretical possibility to further increase the detector efficiency. For example, for a

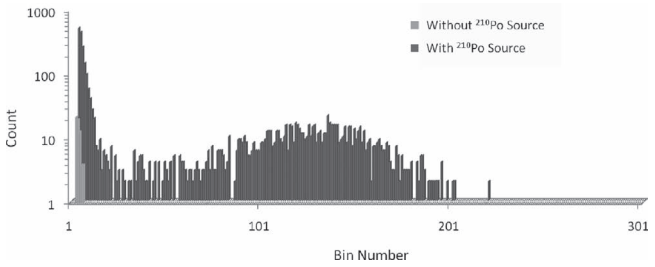

Figure 6. Waterfall plot of the MCA spectra for a solution-processed p-n junction containing 40% $^{10}B_2O_3$ in the top ^{114}CdS layer measured with and without being exposed to the ^{210}Po source. The device was operating with a 0 V bias and the spectrum was collected over a period of 300 s.

$^{114}CdS:^{10}B_2O_3$/Si detector with a top active layer thickness of 50 μm and volume content of the $^{10}B_2O_3$ component of 50%, we estimate the capture cross-section of thermal neutrons to be 27%. Thus, the main remaining challenge in the development of efficient neutron detector is to further improve the carrier transport in the top detector composite layer, so that the overall thickness of this layer could be increased while maintaining efficient collection of the charged carriers.

3. Conclusions

In summary, we have demonstrated utilization of solution-based fabrication of a solid-state p-n junction for radiation detection. As applied to neutron-detectors, the solution-based fabrication enables the neutron sensitizing material to be incorporated throughout the semiconductor matrix, thus overcoming the tradeoff between neutron capture efficiency and charge transport that typically constrains the performance of solid-state neutron detectors. The detectors we fabricated exhibit sensitivity to ionizing radiation and thermal neutrons, and the low cost of the in situ semiconductor synthesis and film fabrication facilitates deployment of large area detector arrays that could be used to effectively disrupt illicit trafficking of nuclear materials.

4. Experimental Section

Film Preparation: For the in situ synthesis and fabrication of the detector top active layer $^{114}CdS:^{10}B_2O_3$ film, a precursor solution containing $^{114}CdCl_2$ (0.1 mmol, 99.01%), thiourea (0.1 mmol, 99.95%) and $^{10}B_2O_3$ (99% enriched with ^{10}B) was prepared in a butylamine (0.8 mL) that acts as a solvent and a ligand for nucleating the inorganic semiconductor nanocrystals. The solution was stirred for several minutes in order to dissolve the precursor molecules, and then was used for drop-casting the film onto a freshly etched silicon wafer by HF acid. During the drop-casting of the solution, the Si wafer was held at predetermined temperature of 150 °C for 15 min in order to eliminate the volatile butylamine solvent as well as initiate a nucleation of ^{114}CdS nanocrystals. After deposition, within few minutes the color of the film changed from white to light yellow, indicating the initial formation of the ^{114}CdS nanocrystals. Following this step, the temperature of the Si wafer was elevated to 450 °C in order to accelerate the semiconductor nanocrystals growth and facilitate a sintering process of these nanocrystals; the elevated temperature also facilitated an elimination of the synthesis reaction byproducts. The duration of the second heating process was about 60 min, and visual monitoring indicated that the film appeared initially to melt and then upon continued heating to re-solidify.

Steady-State Photoconductivity Measurements: For the photoconductivity measurements, two 70 nm thick Au planar electrodes were thermally evaporated on top of the composite film surface using a shadow mask and an evaporator located in a glove box. The steady-state photoconductivity measurements were conducted using a tungsten lamp light source that was monochromized and mechanically modulated using a chopper to enable the use of a sensitive lock-in amplifier for the photocurrent measurement. The lock-in amplifier we used was a Stanford Research Systems SR830. A calibrated Si photodiode was used to determine the lamp power spectrum after each photoconductivity spectrum measurement.

Sensitivity to Ionizing Radiation: The response of the solution-processed $^{114}CdS:^{10}B_2O_3$/Si detectors to ionizing radiation was investigated by irradiating them with 5.3 MeV α particles emitted from a ^{210}Po source. Each detector was prepared by first depositing a $^{114}CdS:^{10}B_2O_3$ on the p-doped Si wafer, followed by a deposition of Al metallic electrode on both,

the bottom side of the p-Si wafer and on top the ^{114}CdS:$^{10}B_2O_3$ film. In order to eliminate the possibility of Schottky barrier formation at the p-Si/Al interfacial region, the device was thermally annealed at 450 °C for 30 min (Al film forms an Ohmic contact with CdS).[28] The rate of α particles emitted by the ^{210}Po source was determined by the signal response obtained from mono-crystalline silicon diode detector, and independently by "MONITOR4" ionizing radiation detector. Both of these detectors indicated a similar flux of alpha particles. A charge-sensitive preamplifier converted the charge carriers excited and collected in the detectors into a voltage signal. The output signals of the charge-sensitive preamplifier were filtered and amplified using an amplifier/shaper before being distributed to a multi-channel analyzer-emulator (MCA) to display the number of counts versus a bin number (that corresponds to the voltage signal peak height which is proportional to the number of carriers collected). The rate of single crystal silicon p-n junction was substituted for the solution-processed device, and although the voltage peak heights obtained from the mono-crystalline silicon device were higher, the total number of counts was nearly the same as that obtained from the device fabricated via solution processing. This similar total number of counts in conjunction with measurement of the α particles emission rate of the ^{210}Po source indicated the neutron-sensitized device detection efficiency for these a particles approaches 100%.

Determination of Detector Sensitivity to Thermal Neutron Radiation: The response of solution-processed ^{114}CdS:$^{10}B_2O_3$/Si detectors to thermal neutron radiation was investigated by irradiating them with radiation emitted by a ^{252}Cf source. The ^{252}Cf source was placed in a vessel made of polyethylene with ~3 inch wall thickness that thermalized the energetic neutrons emitted by the source. The ^{114}CdS:$^{10}B_2O_3$/p-Si detector was shielded by 4 inch lead bricks in order to eliminate any response due to the gamma rays emitted by the ^{252}Cf source, and the pulses generated in the ^{114}CdS:$^{10}B_2O_3$/p-Si detector by the thermal neutrons were detected by a similar system that was used for the detection of ionizing radiation (described above in the section Sensitivity to Ionizing Radiation). ^3He ionization detector was placed near the sample location to verify the presence of neutron radiation.

Supporting Information

Supporting Information is available from the Wiley Online Library or from the author.

Acknowledgements

H.Q.Z. and N.E.C. contributed equally to this work. This research was supported by a DHS grant 2009-DN-077-ARI 028-03 (Dr. Mark Wrobel, program manager). D.M. is grateful to Dr. Thomas E. Old for introducing him to the field of neutron detection; this author is also grateful to Dr. Thomas E. Old, John Baker, Dr. Neal Carron, Dr. Ivan Lorkovic, Dr. John T. Bays, and Dr. Peter C. Ford for initial collaboration in this field.

Received: January 12, 2012
Revised: March 10, 2012
Published online: April 25, 2012

[1] W. K. Hagan, Caught by Surprise: Causes and Consequences of the Helium-3 Supply Crisis *House Committee on Science and Technology, Subcommittee on Investigations and Oversight* **2010**.
[2] M. L. Wald, *The New York Times* **2011**, A25.
[3] G. Aloise, Recent Testing Raises Issues About the Potential Effectiveness of Advanced Radiation Detection Portal Monitors, *GAO-10-252T*, **2009**.
[4] S. E. Flynn, *Foreign Affairs* **2000**, *79*, 57.
[5] An act passed the United States House of representatives, H. R. 4954, *Section 121*, **2006**.
[6] G. F. Knoll, *Radiation Detection and Measurement*, Wiley, University of Michigan, Ann Arbor **2000**.
[7] A. Rose, *Nucl. Instrum. Methods* **1967**, *52*, 166.
[8] F. Shiraishi, Y. Takami, T. Hashimoto, K. Hatori, *IEEE Trans. Nucl. Sci.* **1988**, *35*, 575.
[9] C. Petrillo, F. Sacchetti, O. Toker, N. J. Rhodes, *Nucl. Instrum. Methods A* **1996**, *378*, 541.
[10] R. J. Nikolic, C. L. Cheung, C. E. Reinhardt, T. F. Wang, J. Piprek, *Proc. SPIE*, **2005**, *6013*, 601305.
[11] J. K. Shultis, D. S. McGregor, *IEEE Trans. Nucl. Sci.* **2006**, *53*, 1659.
[12] R. J. Nikoli, A. M. Conway, C. E. Reinhardt, R. T. Graff, T. F. Wang, N. Deo, C. L. Cheung, *Appl. Phys. Lett.* **2008**, *93*, 133502.
[13] R. J. Nikoli, A. M. Conway, R. Radev, Q. Shao, L. F. Voss, T. F. Wang, J. R. Brewer, C. L. Cheung, L. Fabris, C. L. Britton, M. N. Ericsson, *Proc. SPIE* **2010**, *7805*, 78050O.
[14] A. M. Conway, T. F. Wang, N. Deo, C. L. Cheung, R. J. Nikolic, *IEEE Trans. Nucl. Sci.* **2009**, *56*, 2802.
[15] C. B. Murray, M. G. Bawendi, *Abstr Pap Am Chem S* **1993**, *205*, 136.
[16] D. J. Milliron, S. M. Hughes, Y. Cui, L. Manna, J. Li, L. W. Wang, A. P. Alivisatos, *Nature* **2004**, *430*, 190.
[17] I. Gur, N. A. Fromer, M. L. Geier, A. P. Alivisatos, *Science* **2005**, *310*, 462.
[18] C. R. Kagan, D. B. Mitzi, C. D. Dimitrakopoulos, *Science* **1999**, *286*, 945.
[19] V. Sukhovatkin, S. Hinds, L. Brzozowski, E. H. Sargent, *Science* **2009**, *324*, 1542.
[20] Q. Guo, S. J. Kim, M. Kar, W. N. Shafarman, R. W. Birkmire, E. A. Stach, R. Agrawal, H. W. Hillhouse, *Nano Lett.* **2008**, *8*, 2982.
[21] G. Konstantatos, I. Howard, A. Fischer, S. Hoogland, J. Clifford, E. Klem, L. Levina, E. H. Sargent, *Nature* **2006**, *442*, 180.
[22] D. V. Talapin, C. B. Murray, *Science* **2005**, *310*, 86.
[23] L. Li, N. Coates, D. Moses, *J. Am. Chem. Soc.* **2010**, *132*, 22.
[24] N. E. Coates, H. Zhou, S. Kraemer, L. Li, D. Moses, *Adv. Mater.* **2010**, *22*, 5366.
[25] C. Coluzza, M. Garozzo, G. Maletta, D. Margadonna, R. Tomaciello, P. Migliorato, *Appl. Phys. Lett.* **1980**, *37*, 569.
[26] T. Hayashi, T. Nishikura, K. Nishimura, Y. Ema, *Jpn. J. Appl. Phys.* **1989**, *28*, 1174.
[27] A. N. Goldstein, C. M. Echer, A. P. Alivisatos, *Science* **1992**, *256*, 1425.
[28] Z. J. Horváth, M. Ádám, I. Szabó, M. Serényi, V. V. Yuyen, *Appl. Surf. Sci.* **2002**, *190*, 441.